ACS APPLIED MATERIALS & INTERFACES

Research Article

www.acsami.org

Nitrogen-Doped Graphene with Pyridinic Dominance as a Highly Active and Stable Electrocatalyst for Oxygen Reduction

Jingjie Wu,‡ Lulu Ma,‡ Ram Manohar Yadav, Yingchao Yang, Xiang Zhang, Robert Vajtai, Jun Lou,* and Pulickel M. Ajayan*

Department of Material Science and NanoEngineering, Rice University, Houston, Texas 77005, United States

Supporting Information

ABSTRACT: The nitrogen-doped graphene (NG) with dominance of the pyridinic-N configuration is synthesized via a straightforward process including chemical vapor deposition (CVD) growth of graphene and postdoping with a solid nitrogen precursor of graphitic C_3N_4 at elevated temperature. The NG fabricated from CVD-grown graphene contains a high N content up to 6.5 at. % when postdoped at 800 °C but maintains high crystalline quality of graphene. The obtained NG exhibits high activity, long-standing stability, and outstanding crossover resistance for electrocatalysis of oxygen reduction reaction (ORR) in alkaline medium. The NG treated at 800 °C shows the best ORR performance. Further study of the dependence of ORR activity on different N functional groups in these metal-free NG electrodes provides deeper insights into the origin of ORR activity. Our results reveal that the pyridinic-N tends to be the most active N functional group to facilitate ORR at low overpotential via a four-electron pathway.

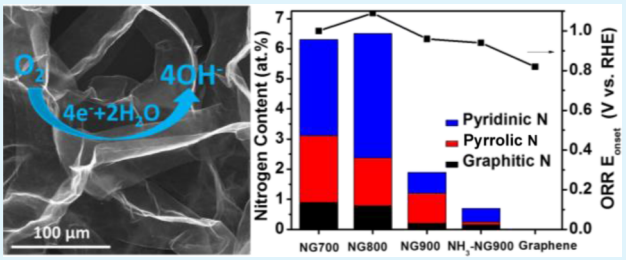

KEYWORDS: *nitrogen-doped graphene, low defect, metal-free, nitrogen functionality, pyridinic nitrogen, oxygen reduction reaction*

INTRODUCTION

The high required overpotential and sluggish kinetics of the oxygen reduction reaction (ORR) is the primary cause of potential loss in both alkaline and proton exchange membrane fuel cells. The contemporarily used catalyst platinum (Pt) for ORR suffers from its scarcity and susceptibility to CO poisoning.[1,2] As a result, the search of alternatives to Pt has drawn immense attention in the field of electrocatalysis. The heteroatom (mostly nitrogen, N)-doped carbon nanostructures emerge as promising candidates due to their excellent activity toward ORR especially in alkaline electrolyte, high stability, and resistivity toward CO or methanol poisoning.[3−7]

The N incorporates into the carbon network with bonding configurations of the N atom in six-membered rings (pyridinic-N), five-membered rings (pyrrolic-N), graphene basal plane (graphitic/quaternary-N_{center}), graphene zigzag edge or valley sites (graphitic-N_{valley}), and bonding to O atoms (oxidized nitrogen species).[8−11] However, the role of different N functional groups in the electrocatalysis of ORR is still under debate in results from theoretical calculation and experimental measurement since the first exploration of nitrogen-doped carbon nanotubes (N-CNTs) as active ORR catalysts.[3,4,10] Most of the previous work did not distinguish between graphitic-N_{center} and graphitic-N_{valley} and just proclaimed that the graphitic N was of paramount importance for the ORR activity.[12−14] The graphitic-N_{center} geometry mostly enhances the O_2 adsorption onto the adjacent C and breaks the O−O bond easier to reduce O_2 via a four-electron reduction pathway.[9] On the other hand, some work reported no contribution from graphitic-N_{center} and asserted that the electrocatalytic activity mainly comes from three N configurations in the edge planes, including pyridinic-N, pyrrolic-N, and graphitic N_{valley}.[8] Nonetheless, the explicit active site is still contentious between the pyridinic-N and graphitic-N_{valley}.[8,14−18] The graphitic-N_{valley} promotes the ORR activity, whereas pyridinic N suppresses the ORR activity, as claimed by some researchers.[19] Density functional theory (DFT) modeling shows that graphitic-N_{valley} lowers the adsorption energy of oxygen and facilitates the first electron transfer; however, the ORR is catalyzed through a ring-opening process of the cyclic C−N bond, resulting in the formation of pyridinic-N.[14] In contrast, many other papers stated that pyridinic-N does not suppress but facilitates the ORR activity.[17,20−26] The calculation through DFT also shows that pyridinic-N enhances O_2 adsorption on the neighboring carbon atoms by inducing high spin density and positive atomic charge density to the neighboring carbon atoms and thus promotes a four-electron process of ORR.[27] The introduction of a trace transition metal such as Fe during the synthesis of CNTs adds additional complexity to the exploration of N active sites in the N-CNTs, since Fe tends to form a F−N bond, which was revealed to be highly active in the electrocatalysis of ORR.[5] Moreover, it is also difficult to rule out the other effects such as the tube diameter and number of walls of N-CNTs on the activity.

Received: April 2, 2015
Accepted: June 19, 2015
Published: June 19, 2015

DOI: 10.1021/acsami.5b02902
ACS Appl. Mater. Interfaces 2015, 7, 14763−14769

Graphene (G) possesses the unique graphitic basal plane structure which could further facilitate the electron transport, while having many similarities with CNTs in chemical and physical properties.[4,28] However, like CNTs, the exploration results of actual N active sites based on N-doped reduced graphene oxides (N-rGO) also involve the effect of metals (Fe and Mn) when prepared from the Staudenmaier and Hummers oxidation method, respectively.[12,29] Additionally, the graphite, as the source material for rGO, contains trace amounts of transition metals, such as Fe, Co, Ni, and Mn, making the exploration complicated. With this in mind, instead of choosing CNTs and rGOs, we use few-layer graphene grown by chemical vapor deposition (CVD) as the starting carbon material, which possesses negligible defects compared to CNTs and rGOs. Herein, we have demonstrated a straightforward postdoping of CVD-grown high-quality few-layer graphene by a simple method of annealing graphene with graphitic carbon nitride (g-C_3N_4) at elevated temperature. In situ doping of graphene was not chosen because nitrogen present in in situ doping reacts with metal substrates and hinders the growth of high-quality graphene. Our process combining CVD-growth and postdoping eliminates the possibility of introducing strongly active trace metals such as Fe and Mn from either the source materials or the synthesis catalysts. The as-prepared N-doped graphene (NG) was used to further explore the role of nitrogen functional groups in the electrocatalysis of ORR. In addition, superior to CNTs and rGOs, the CVD-grown graphene facilitates electron transport due to its two-dimensional (2D) planar geometry and low defect level and, hence, could be a more effective electrode material. Our study provides deeper insights into the ORR mechanism of N active sites in NG and demonstrates a feasible method to fabricate non-noble metal-free ORR catalysts with tunable activity.

EXPERIMENTAL SECTION

Materials Synthesis. The three-dimensional (3D) graphene foam was grown by ambient-pressure CVD of methane on Ni foam at 1000 °C with Ar/H_2 purging during the synthesis process. The as-grown graphene was collected by first etching away the Ni substrate in an aqueous solution of HCl, followed by vacuum filtering and washing with deionized water. After drying in a vacuum oven, a certain amount of graphene was dissolved again with assistance of sonication in concentrated HCl (Sigma-Aldrich), followed by centrifuging at 8000 rpm for 5 min. The suspension was taken for atomic absorption spectrometry (AAS, PerkinElmer's PinAAcle 500) measurement. The AAS shows that the suspension has a very similar Ni concentration to that of the solvent HCl only suggesting negligible Ni remaining in our graphene samples. The CVD-grown graphene was then postdoped using either a solid precursor g-C_3N_4 or a gas precursor NH_3 at the temperature range of 700−900 °C to obtain NG.

Physical Characterizations. The microstructures of NG were analyzed by electron microscopy including a scanning electron microscope (SEM, FEI Quanta 400) and a transmission electron microscope (TEM, JEOL 2100). The disorder of NG was evaluated by Raman spectroscopy with a laser excitation of 514.5 nm. The N content and configuration were analyzed by X-ray photoelectron spectroscopy (XPS, PHI Quanter XPS with Al Kα X-ray). The Brunauer−Emmett−Teller (BET) surface area was obtained by the N_2 adsorption/desorption measurement at 77 K using a NOVA 4200e (Quantachrome). The surface area for pristine graphene from BET calculation is around 830 m^2/g, close to that of other reported 3D graphene foams.[30]

Electrochemical Measurement. The electrochemical activity was measured in a rotating ring-disk electrode (RRDE) (disk glassy carbon diameter: 5 mm, Pine Research Instrument) with a CHI 760D potentiostat. The catalyst ink was prepared by ultrasonicating the mixture of 1 mg of pristine graphene or NG, 125 μL of DI water, 75 μL of 2-propanol, and 20 μL of Nafion dispersion (0.5 wt %) for 30 min. For comparison, a catalyst ink with 1 mg/220 μL commercial Pt/C (20 wt %, Johnson Matthew) was also prepared using the same procedure described above; 8 μL of the catalyst ink was pipetted to cover the disk electrode surface. After the ink dries at room temperature, a 5 μL Nafion dispersion (0.5 wt %) was dropped onto the electrode surface. This leads to a catalyst loading of 180 μg cm^{-2} for pristine graphene and NG samples while 36 μg cm^{-2} for Pt. The RRDE loaded with the catalysts was employed as the working electrode, while a Ag/AgCl (saturated KCl) electrode was used as the reference electrode and a Pt foil (0.5 cm × 3 cm) served as the counter electrode. All the potential was referred to a reversible hydrogen electrode (RHE), $E_{RHE} = E_{Ag/AgCl} + 0.20\ V + 0.0591pH$.

Cyclic voltammetric study was performed at 50 mV s^{-1} in either Ar- or O_2-saturated electrolyte of 0.1 M KOH. The RRDE was measured in O_2 bubbling 0.1 M KOH by sweeping the disk potential negatively from 1.2 to 0 V at 5 mV s^{-1}. The ring potential was maintained at 1.25 V in order to reverse the reaction by oxidizing the intermediate product. The presented linear sweep curve data in Ar-saturated electrolyte was subtracted from that in O_2 bubbling electrolyte to remove the capacitance effect. Two tangents from the rising and background current of the linear potential sweeping curve intersect at which the onset potential is determined. Regarding the measurement of crossover resistance, the chronoamperometry was carried out at −0.57 V in 0.1 M KOH containing 0.5 M methanol. The accelerated stability test was conducted by cycling the potential between 0.4 and 1.0 V for 5000 cycles.

The number of electrons transferred per oxygen molecule (n) was extracted from the Koutecký-Levich (K−L) equation

$$\frac{1}{j} = \frac{1}{j_k} + \frac{1}{j_d} = \frac{1}{nFkC_{O_2}^b} + \frac{1}{0.2nFD_{O_2}^{2/3}\nu^{-1/6}C_{O_2}^b\omega^{1/2}} \quad (1)$$

where j, j_k, and j_d are the measured, kinetic, and diffusion-limiting current densities, respectively, and ω is the RRDE rotation speed with a unit of rpm. The other parameters have their common physical meaning, and the values can be found in previous reports.[15,31] The transferred electron numbers can be determined alternatively from the ratio of ring current over disk current.[10]

$$n = \frac{4I_D}{I_D + \frac{I_R}{N}} \quad (2)$$

RESULTS AND DISCUSSION

To boost the active surface area for catalyzing oxygen reduction, 3D graphene foam was grown by ambient-pressure CVD of methane on Ni foam.[32] The as-grown graphene foam was then postdoped using a solid precursor g-C_3N_4 to enhance the doping content of nitrogen. A typical microstructure of NG doped at 800 °C (denoted as NG-800) is shown in SEM images (Figure 1). Figure 1a shows the interlocked 3D structure of NG with all the NG sheets in good contact with one another. Figure 1b shows the morphology of NG sheets with a smooth surface and electron transparency. The high-resolution TEM shows that NG consists of mono- to few-layer NG sheets (Figure 1c and Figure S1, Supporting Information). The hexagonal patterns of graphene were observed in NG, indicating that the main carbon sp^2 structure is maintained after incorporation of N heteroatoms under our doping conditions (Figure 1c).

Raman spectra were taken on NG at the doping temperature of 700−900 °C and a pristine graphene for reference. The spectrum for pristine graphene shows only G and 2D bands at 1583 and 2710 cm^{-1}, respectively. The pristine graphene lacks a D peak associated with the point defects such as single or double carbon vacancies in the graphene lattice, implying a

DOI: 10.1021/acsami.5b02902
ACS Appl. Mater. Interfaces 2015, 7, 14763−14769

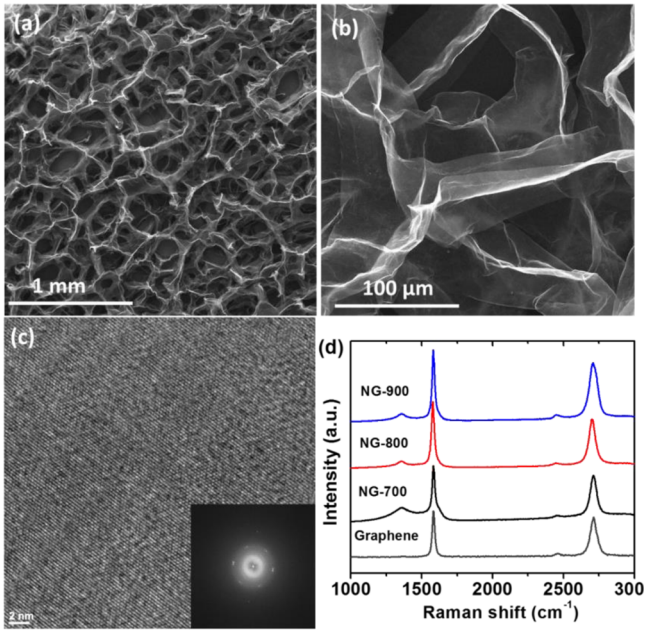

Figure 1. Morphology and microstructure of N-doped graphene. (a, b) SEM images of NG-800. (c) High-resolution TEM image of NG-800, and inset is the fast Fourier transform showing the hexagonal symmetric structure. (d) Raman spectra of N-doped and pristine graphene.

perfect six-atom ring lattice in the CVD-grown graphene (Figure 1d).[33] In contrast, previous work reported a noticeable defect-related D peak for both pristine CNTs and rGO, leading to the hindered electron transport compared to the CVD-grown graphene.[10,12] Raman spectra of NGs show a tiny D peak at 1353 cm^{-1} attributed to the little structural distortion caused by N-doping. The small ratio of D to G band intensity of 0.1−0.2 (Figure S2, Supporting Information) suggests that NG maintains a very good crystalline structure, in agreement with the TEM results. The intensity ratio of G over 2D band reveals that NG has 2−4 layers.[4,34]

The surface content and chemical states of N were identified by XPS. The survey spectra of NGs clearly show a peak at 400 eV for N in addition to a dominant graphitic C peak at 284.5 eV (Figure S3, Supporting Information). Importantly, no peaks for transitional metals Ni, Fe, and Mn are found in the spectra. The high-resolution asymmetric peak of C 1s was fitted into a core peak of the C═C bond (284.5 eV), and four satellite peaks corresponding to the C═N bond (285.2 eV), C−C bond (285.5 eV), C−N bond (286.2 eV), and C−O bond (286.7 eV), indicating successful incorporation of heteroatom N into the graphene hexagonal plane (Figure S3).[15,35] The deconvolution of the N 1s XPS peak reveals three different N configurations at 398.45, 400.06, and 401.20 eV, assigned to the pyridinic-N (N1), pyrrolic-N (N2), and graphitic-N_{center} (N3), respectively (Figure 2a,c).[10,15] The graphitic-N_{valley} in the valley sites (N4) with binding energy > 402 eV is not found in our NGs.[10,11] The total surface N content as calculated from N/(N + C) atomic ratio is higher at lower doping temperature, e.g., the NG-700 °C with 6.3 at. % N vs NG-900 with 1.9 at. % (Figure 2b; Table S1, Supporting Information). The drop of N content probably resulted from the elimination of some unstable N moieties like pyridinic-N and pyrrolic-N at high temperature, consistent with previous findings.[10,36,37] For comparison, we also used a gas precursor NH_3 to dope graphene at 900 °C (denoted as NH_3-NG-900). NH_3 leads to much lower N content compared with the solid precursor g-C_3N_4 (Figure S3 and Table S1). Pyridinic-N predominates in all NGs except for NG-900 with the pyrrolic-N dominance (Figure 2b and Figure S4, Supporting Information).

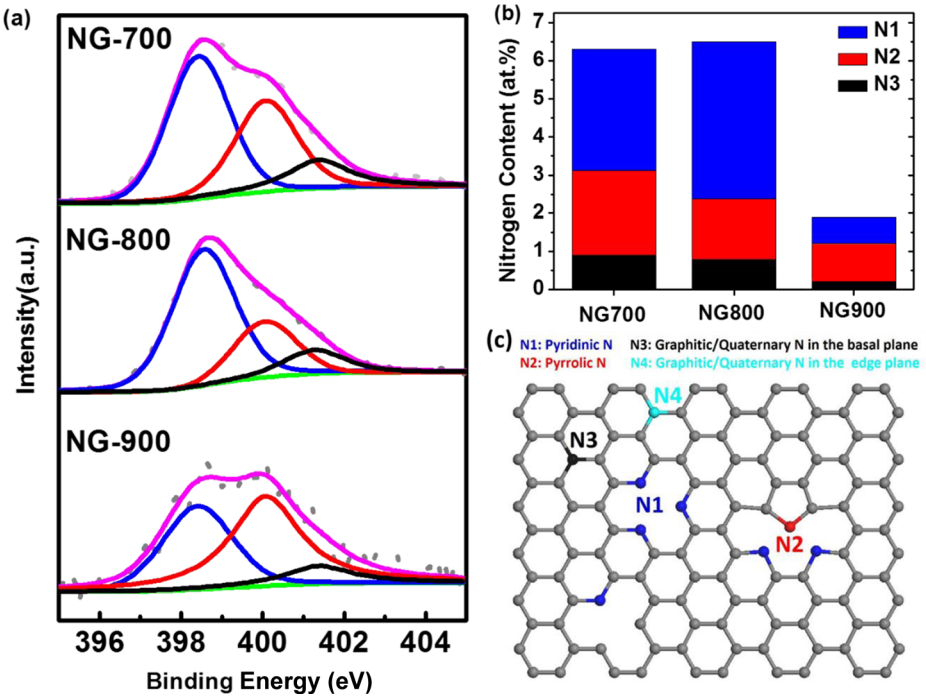

Figure 2. X-ray photoelectron spectra of nitrogen-doped graphene. (a) High-resolution XPS scan for N 1s core level peak. The peaks are deconvoluted into component curves. (b) N functionality distribution obtained from the peak area ratio of N/(N + C). (c) The schematic of different N functional groups incorporated in the graphene plane.

DOI: 10.1021/acsami.5b02902
ACS Appl. Mater. Interfaces 2015, 7, 14763−14769

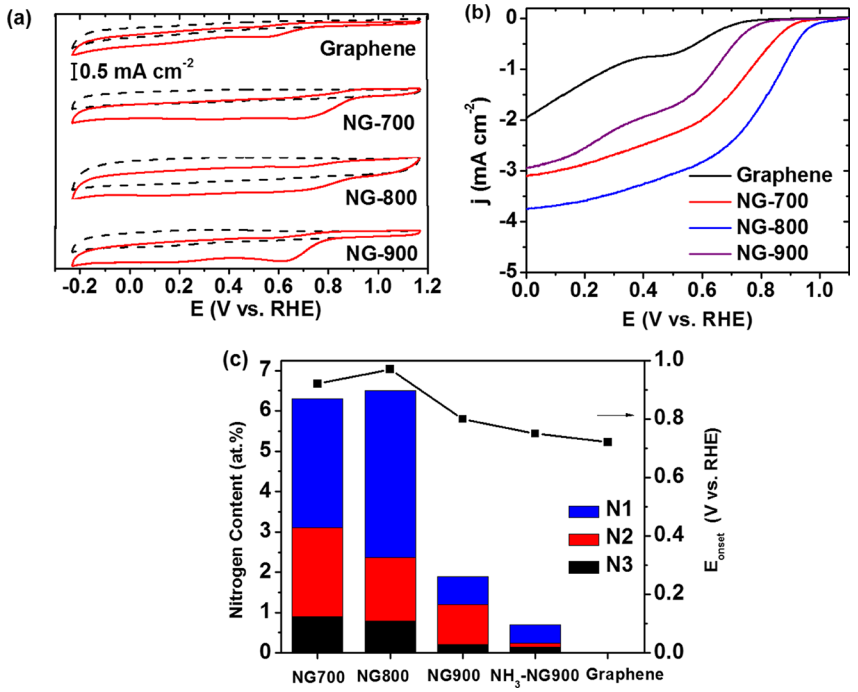

Figure 3. Electrocatalytic activity toward ORR of graphene and N-doped graphene. (a) Cyclic voltammetries in O_2-saturated (solid) and Ar-saturated (dotted) 0.1 M KOH. (b) RDE polarization curves in O_2-saturated 0.1 M KOH. Electrode rotation speed, 900 rpm; scan rate, 5 mV s^{-1}; room temperature. (c) The dependence of onset potential on the N functionality distribution. The data of NH_3-NG-900 are also included.

The comparison studies of ORR activity among these NGs were performed by a rotating ring-disk electrode (RRDE) in O_2-saturated 0.1 M KOH. Cyclic voltammetry measurements show that the peak reduction potential for ORR shifts positively for NG compared to the pristine graphene. The NG-800 has the most positive peak reduction potential, followed by NG-700 and NG-900 (Figure 3a). The NH_3-NG-900 has the most negative peak reduction potential among these NGs due to the lowest nitrogen content (Figure S5, Supporting Information). The meso/micropores in the carbon nanostructure can enhance nitrogen-doping during NH_3 activation, leading to a comparable peak potential to that of NG-800.[38] Figure 3b shows the steady-state polarization curves for ORR on pristine graphene and NGs. The pristine graphene and NG-900 showed a two-step process for ORR with the onset potential of about 0.72 and 0.80 V, respectively. The similar two-step process occurs on NH_3-NG-900 (Figure S5, Supporting Information). A one-step process occurs for NG-700 and NG-800 with an onset potential of 0.92 and 0.97 V, respectively. The onset potential of NG-800 is comparable to that of commercial Pt/C (0.99 V, Figure 4d), and more positive than that of sulfur-doped graphene (0.86 V),[39] but slightly lower than that of recently reported carbon hybrid catalysts like carbon nanotube–graphene complexes (1.05 V)[5] and carbon nanotube/nanoparticles (1.16 V).[6] In addition, NG-800 exhibits the highest steady-state diffusion current density. Overall, the NG-800 exhibits the highest activity regarding the most anodic onset potential and the highest diffusion-limiting current density.

The cyclic voltammetry results show similar capacitance of the double layer at the solid–liquid interface among the studied NG and pristine graphene electrodes, which avoids the potential effect of the electrochemical surface area on the performance (Figure S6, Supporting Information). Another key factor determining the ORR activity is the heteroatom N type

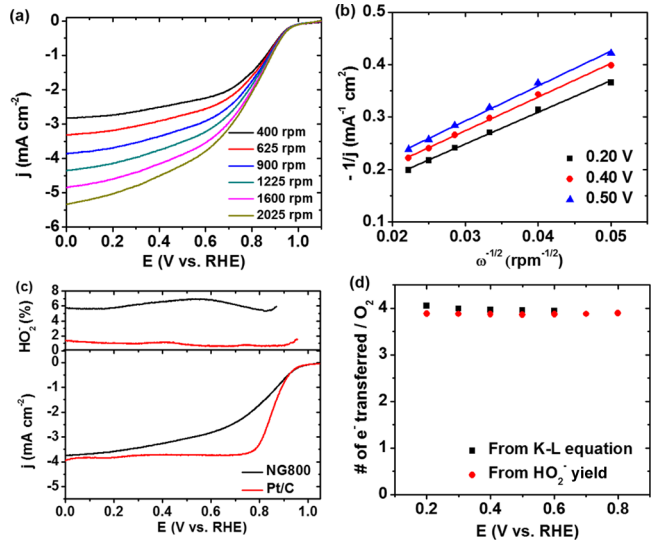

Figure 4. Electrochemical activity toward ORR of N-doped graphene at 800 °C with a comparison to commercial Pt/C. (a) Polarization curves at different rotating speeds. (b) Koutecky–Levich plots. (c) RRDE measurement showing peroxide yield at a rotation rate of 900 rpm. (d) Number of electrons per oxygen molecular transferred during ORR. The electrolyte is O_2-saturated 0.1 M KOH. The polarization scan rate is 5 mV s^{-1}.

and its corresponding atomic concentration since the activity contribution from trace metals can be excluded in our graphene and NG samples. In our NG samples, the contribution of activity comes from at least one of the three N groups (pyridinic-N, pyrrolic-N, and graphitic-N_{center}). The determination of exact active N species is still impossible unless we can achieve the incorporation of a single N functional group in the carbon sp^2 network. The analysis of the N active site was

DOI: 10.1021/acsami.5b02902
ACS Appl. Mater. Interfaces 2015, 7, 14763–14769

carried out by plotting the onset potential versus the N species concentration in Figure 3c. The onset potential shifts more positively along with the increase in pyridinic-N content. The limiting current density also increases with increasing of pyridinic-N content (Figure S7, Supporting Information). These results seem to suggest that the pyridinic-N is likely the most active site for ORR in NG. However, the contribution from pyrrolic-N and graphitic-N_{center} sites could not be excluded based solely on these results. Notably, our NG samples exhibit higher ORR activity than those N-doped CNTs with a high concentration of graphitic-N_{valley}, N-doped rGOs, and N-doped ordered mesoporous graphitic arrays with rich graphitic-N (not distinguishable between N_{center} and N_{valley} in these two cases), further implying that pyridinic-N is more active than graphitic-N.[10,12,40] The calculation through DFT shows that incorporation of pyridinic-N induces the highest spin density and largest positive atomic charge density to the neighboring carbon atoms on which O_2 adsorption is enhanced compared to pyrrolic and graphitic-N.[27] Consequently, the highest activity of NG-800 mainly originates from the highest concentration (4.1 at. %) of pyridinic-N compared to 3.2 at. % for NG-700, 0.70 at. % for NG-900, and 0.45 at. % for NH_3-NG-900.

The activity of NG-800 was investigated in depth. The current density (j) is proportional to the square root of rotating speed (ω) as expected (Figure 4a). Subsequent Koutecký–Levich (K–L) plots j^{-1} vs $\omega^{-1/2}$ at the potential range of the diffusion-controlled regime was plotted (Figure 4b). The linearity of the K–L plots implies first-order reaction kinetics toward the oxygen concentration in the electrolyte.[41] According to the K–L equation, the average electron number (n_e) transferred when reducing one oxygen molecule was calculated to be 3.96–4.05 at the potential range of 0.20–0.50 V.[12,41] The HO_2^- yield is less than 8% at all potentials, decreasing to ~6% at 0.2 V (Figure 4c). The n_e is directly correlated with HO_2^- yield ($n_e = 4 - (\%\ HO_2^-)/50$), which can be calculated from the disk and ring current in the RRDE system. Therefore, n_e is obtained to be 3.86–3.88 between 0.20 and 0.50 V, consistent with the values calculated from the K–L equation (Figure 4d). The n_e for NG-700, NG-900, and NH_3-NG-900 is presented in Figure S8 (Supporting Information). The ORR proceeds mostly via a four-electron pathway on NG-700, whereas it proceeds via a two-electron route on NG-900 and NH_3-NG-900.

The resistance to methanol poisoning was evaluated in 0.1 M KOH containing 0.5 M methanol. The Pt/C is subjected to 70% loss of current after introduction of methanol, as shown in the j–t chronoamperometric response (Figure 5a), while the current for NG-800 remains stable, demonstrating the high selectivity to ORR for the NG-800 electrode. The polarization curves in the presence of methanol also show no loss of activity for the NG-800 electrode. In contrast, a methanol oxidation peak for the Pt/C electrode appears at 0.92 V and a drastic negative shift of potential on the Pt/C electrode is observed due to the mixed potential of ORR and methanol oxidation reaction. The additional j–t chronoamperometric measurement with introducing 10% (v/v) CO into O_2-saturated 0.1 M KOH also shows resistance of the NG-800 electrode to CO poisoning (Figure S9, Supporting Information).

The durability of NG-800 was assessed on the basis of the accelerated durability test protocol. The performance of NG-800 maintains after 5000 cycles (Figure 5d), whereas, for a comparison, Pt/C shifts the half-wave potential ($E_{1/2}$) negatively by 20 mV under the similar test conditions (Figure S10, Supporting Information).

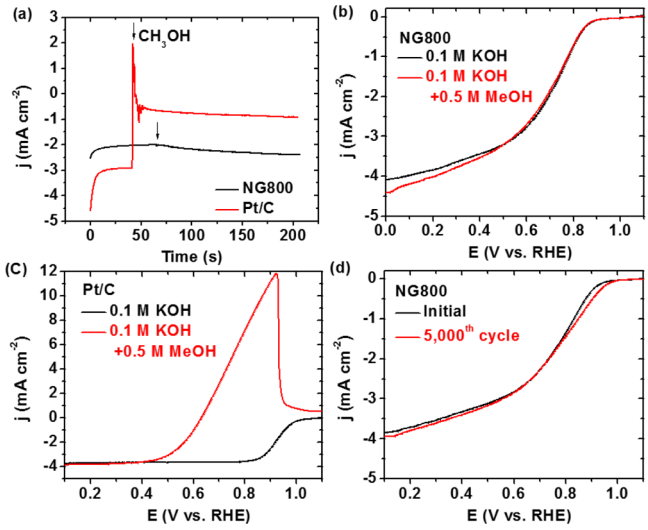

Figure 5. Resistance to methanol poisoning and stability of N-doped graphene at 800 °C. (a) Chronoamperometric response of NG-800 and Pt/C electrodes at 0.56 V vs RHE in O_2-saturated 0.1 M KOH. The arrow indicates the onset addition of 0.5 M methanol into the O_2-saturated electrolyte. (b, c) The RDE polarization curves in the presence or absence of methanol for NG-800 and Pt/C, respectively. (d) RDE polarization curves of NG-800 before and after stability test in O_2-saturated 0.1 M KOH. The polarization curves were measured under 5 mV s^{-1} with a rotating speed of 900 rpm.

CONCLUSIONS

NG can be synthesized by a simple method of annealing CVD-grown graphene with g-C_3N_4 at temperatures from 700 to 900 °C. The concentration and configuration of nitrogen vary with different doping temperatures. These NGs, which originated from low defect CVD-grown graphene, contain a high N concentration up to 6.5 at. % without sacrificing the quality of graphene. The NG electrodes exhibit high activity, long-standing stability, and superior crossover resistance for the electrocatalysis of ORR. The activity of NGs is tunable via controlling the nitrogen-doping concentration and configuration. It was found that NG doped at 800 °C shows the best ORR performance and exhibits similar onset potential with Pt catalyst. The ORR at NG doped at 700 and 800 °C proceeds via a four-electron process, whereas it shifts to a two-electron process for NG doped at the increased temperature of 900 °C. The analysis of our results suggests that the pyridinic-N tends to be the most active N functional group to facilitate ORR proceeding at low overpotential.

ASSOCIATED CONTENT

Supporting Information

More materials characterization of NG and graphene, cyclic voltagramms of NG and graphene, yield of HO_2^- for NG electrodes, and stability of Pt/C. The Supporting Information is available free of charge on the ACS Publications website at DOI: 10.1021/acsami.5b02902.

AUTHOR INFORMATION

Corresponding Authors

*E-mail: jlou@rice.edu (J.L.).
*E-mail: ajayan@rice.edu (P.M.A.).

DOI: 10.1021/acsami.5b02902
ACS Appl. Mater. Interfaces 2015, 7, 14763–14769

Author Contributions

‡These authors contributed equally. The manuscript was written through contributions from J.W., L.M., and R.M.Y. All authors have given approval to the final version of the manuscript.

Notes

The authors declare no competing financial interests.

■ ACKNOWLEDGMENTS

J.W. and L.M. thank the U.S. Air Force Office of Scientific Research (Award FA9550-14-1-0268) for the funding support. R.M.Y. thanks the University Grants Commission, Government of India, for the Raman Fellowship. J.L. and Y.Y. are thankful for the Welch foundation grant C-1716.

■ REFERENCES

(1) Gasteiger, H. A.; Kocha, S. S.; Sompalli, B.; Wagner, F. T. Activity Benchmarks and Requirements for Pt, Pt-alloy, and Non-Pt Oxygen Reduction Catalysts for PEMFCs. *Appl. Catal., B* **2005**, *56*, 9−35.

(2) Wu, J.; Yang, H. Platinum-Based Oxygen Reduction Electrocatalysts. *Acc. Chem. Res.* **2013**, *46*, 1848−1857.

(3) Gong, K.; Du, F.; Xia, Z.; Durstock, M.; Dai, L. Nitrogen-Doped Carbon Nanotube Arrays with High Electrocatalytic Activity for Oxygen Reduction. *Science* **2009**, *323*, 760−764.

(4) Qu, L.; Liu, Y.; Baek, J.-B.; Dai, L. Nitrogen-Doped Graphene as Efficient Metal-Free Electrocatalyst for Oxygen Reduction in Fuel Cells. *ACS Nano* **2010**, *4*, 1321−1326.

(5) Li, Y.; Zhou, W.; Wang, H.; Xie, L.; Liang, Y.; Wei, F.; Idrobo, J.-C.; Pennycook, S. J.; Dai, H. An Oxygen Reduction Electrocatalyst Based on Carbon Nanotube-Graphene Complexes. *Nat. Nano.* **2012**, *7*, 394−400.

(6) Chung, H. T.; Won, J. H.; Zelenay, P. Active and Stable Carbon Nanotube/Nanoparticle Composite Electrocatalyst for Oxygen Reduction. *Nat. Commun.* **2013**, *4*, 1922.

(7) Yang, D.-S.; Bhattacharjya, D.; Inamdar, S.; Park, J.; Yu, J.-S. Phosphorus-Doped Ordered Mesoporous Carbons with Different Lengths as Efficient Metal-Free Electrocatalysts for Oxygen Reduction Reaction in Alkaline Media. *J. Am. Chem. Soc.* **2012**, *134*, 16127−16130.

(8) Biddinger, E. J.; Ozkan, U. S. Role of Graphitic Edge Plane Exposure in Carbon Nanostructures for Oxygen Reduction Reaction. *J. Phys. Chem. C* **2010**, *114*, 15306−15314.

(9) Lai, L.; Potts, J. R.; Zhan, D.; Wang, L.; Poh, C. K.; Tang, C.; Gong, H.; Shen, Z.; Lin, J.; Ruoff, R. S. Exploration of the Active Center Structure of Nitrogen-Doped Graphene-Based Catalysts for Oxygen Reduction Reaction. *Energy Environ. Sci.* **2012**, *5*, 7936−7942.

(10) Sharifi, T.; Hu, G.; Jia, X.; Wågberg, T. Formation of Active Sites for Oxygen Reduction Reactions by Transformation of Nitrogen Functionalities in Nitrogen-Doped Carbon Nanotubes. *ACS Nano* **2012**, *6*, 8904−8912.

(11) Ouyang, W.; Zeng, D.; Yu, X.; Xie, F.; Zhang, W.; Chen, J.; Yan, J.; Xie, F.; Wang, L.; Meng, H.; Yuan, D. Exploring the Active Sites of Nitrogen-Doped Graphene as Catalysts for the Oxygen Reduction Reaction. *Int. J. Hydrogen Energy* **2014**, *39*, 15996−16005.

(12) Geng, D.; Chen, Y.; Chen, Y.; Li, Y.; Li, R.; Sun, X.; Ye, S.; Knights, S. High Oxygen-Reduction Activity and Durability of Nitrogen-Doped Graphene. *Energy Environ. Sci.* **2011**, *4*, 760−764.

(13) Nagaiah, T. C.; Kundu, S.; Bron, M.; Muhler, M.; Schuhmann, W. Nitrogen-Doped Carbon Nanotubes as a Cathode Catalyst for the Oxygen Reduction Reaction in Alkaline Medium. *Electrochem. Commun.* **2010**, *12*, 338−341.

(14) Kim, H.; Lee, K.; Woo, S. I.; Jung, Y. On the Mechanism of Enhanced Oxygen Reduction Reaction in Nitrogen-Doped Graphene Nanoribbons. *Phys. Chem. Chem. Phys.* **2011**, *13*, 17505−17510.

(15) Ratso, S.; Kruusenberg, I.; Vikkisk, M.; Joost, U.; Shulga, E.; Kink, I.; Kallio, T.; Tammeveski, K. Highly Active Nitrogen-Doped Few-Layer Graphene/Carbon Nanotube Composite Electrocatalyst for Oxygen Reduction Reaction in Alkaline Media. *Carbon* **2014**, *73*, 361−370.

(16) Zhang, Y.; Fugane, K.; Mori, T.; Niu, L.; Ye, J. Wet Chemical Synthesis of Nitrogen-Doped Graphene towards Oxygen Reduction Electrocatalysts without High-Temperature Pyrolysis. *J. Mater. Chem.* **2012**, *22*, 6575−6580.

(17) Liu, M.; Song, Y.; He, S.; Tjiu, W. W.; Pan, J.; Xia, Y.-Y.; Liu, T. Nitrogen-Doped Graphene Nanoribbons as Efficient Metal-Free Electrocatalysts for Oxygen Reduction. *ACS Appl. Mater. Interfaces* **2014**, *6*, 4214−4222.

(18) Wiggins-Camacho, J. D.; Stevenson, K. J. Mechanistic Discussion of the Oxygen Reduction Reaction at Nitrogen-Doped Carbon Nanotubes. *J. Phys. Chem. C* **2011**, *115*, 20002−20010.

(19) Niwa, H.; Horiba, K.; Harada, Y.; Oshima, M.; Ikeda, T.; Terakura, K.; Ozaki, J.-i.; Miyata, S. X-ray Absorption Analysis of Nitrogen Contribution to Oxygen Reduction Reaction in Carbon Alloy Cathode Catalysts for Polymer Electrolyte Fuel Cells. *J. Power Sources* **2009**, *187*, 93−97.

(20) Xing, T.; Zheng, Y.; Li, L. H.; Cowie, B. C. C.; Gunzelmann, D.; Qiao, S. Z.; Huang, S.; Chen, Y. Observation of Active Sites for Oxygen Reduction Reaction on Nitrogen-Doped Multilayer Graphene. *ACS Nano* **2014**, *8*, 6856−6862.

(21) Chen, Z.; Higgins, D.; Tao, H.; Hsu, R. S.; Chen, Z. Highly Active Nitrogen-Doped Carbon Nanotubes for Oxygen Reduction Reaction in Fuel Cell Applications. *J. Phys. Chem. C* **2009**, *113*, 21008−21013.

(22) Rao, C. V.; Cabrera, C. R.; Ishikawa, Y. In Search of the Active Site in Nitrogen-Doped Carbon Nanotube Electrodes for the Oxygen Reduction Reaction. *J. Phys. Chem. Lett.* **2010**, *1*, 2622−2627.

(23) Chang, D. W.; Choi, H.-J.; Baek, J.-B. Wet-Chemical Nitrogen-Doping of Graphene Nanoplatelets as Electrocatalysts for the Oxygen Reduction Reaction. *J. Mater. Chem. A* **2015**, *3*, 7659−7665.

(24) Vikkisk, M.; Kruusenberg, I.; Joost, U.; Shulga, E.; Kink, I.; Tammeveski, K. Electrocatalytic Oxygen Reduction on Nitrogen-Doped Graphene in Alkaline Media. *Appl. Catal., B* **2014**, *147*, 369−376.

(25) Wu, G.; Mack, N. H.; Gao, W.; Ma, S.; Zhong, R.; Han, J.; Baldwin, J. K.; Zelenay, P. Nitrogen-Doped Graphene-Rich Catalysts Derived from Heteroatom Polymers for Oxygen Reduction in Nonaqueous Lithium-O_2 Battery Cathodes. *ACS Nano* **2012**, *6*, 9764−9776.

(26) Yadav, R. M.; Wu, J.; Kochandra, R.; Ma, L.; Tiwary, C. S.; Ge, L.; Ye, G.; Vajtai, R.; Lou, J.; Ajayan, P. M. Carbon Nitrogen Nanotubes as Efficient Bifunctional Electrocatalysts for Oxygen Reduction and Evolution Reactions. *ACS Appl. Mater. Interfaces* **2015**, *7*, 11991−2000.

(27) Zhang, L.; Xia, Z. Mechanisms of Oxygen Reduction Reaction on Nitrogen-Doped Graphene for Fuel Cells. *J. Phys. Chem. C* **2011**, *115*, 11170−11176.

(28) Geim, A. K. Graphene: Status and Prospects. *Science* **2009**, *324*, 1530−1534.

(29) Wang, L.; Ambrosi, A.; Pumera, M. "Metal-Free" Catalytic Oxygen Reduction Reaction on Heteroatom-Doped Graphene is Caused by Trace Metal Impurities. *Angew. Chem., Int. Ed.* **2013**, *52*, 13818−13821.

(30) Yavari, F.; Chen, Z.; Thomas, A. V.; Ren, W.; Cheng, H.-M.; Koratkar, N. High Sensitivity Gas Detection Using a Macroscopic Three-Dimensional Graphene Foam Network. *Sci. Rep.* **2011**, *1*, 166.

(31) Davis, R. E.; Horvath, G. L.; Tobias, C. W. The Solubility and Diffusion Coefficient of Oxygen in Potassium Hydroxide Solutions. *Electrochim. Acta* **1967**, *12*, 287−297.

(32) Chen, Z.; Ren, W.; Gao, L.; Liu, B.; Pei, S.; Cheng, H. M. Three-Dimensional Flexible and Conductive Interconnected Graphene Networks Grown by Chemical Vapor Deposition. *Nat. Mater.* **2011**, *10*, 424−8.

(33) Cançado, L. G.; Jorio, A.; Ferreira, E. H. M.; Stavale, F.; Achete, C. A.; Capaz, R. B.; Moutinho, M. V. O.; Lombardo, A.; Kulmala, T. S.; Ferrari, A. C. Quantifying Defects in Graphene via Raman

DOI: 10.1021/acsami.5b02902
ACS Appl. Mater. Interfaces 2015, 7, 14763−14769

Spectroscopy at Different Excitation Energies. *Nano Lett.* **2011**, *11*, 3190−3196.
(34) Hao, Y.; Wang, Y.; Wang, L.; Ni, Z.; Wang, Z.; Wang, R.; Koo, C. K.; Shen, Z.; Thong, J. T. L. Probing Layer Number and Stacking Order of Few-Layer Graphene by Raman Spectroscopy. *Small* **2010**, *6*, 195−200.
(35) Sheng, Z.-H.; Shao, L.; Chen, J.-J.; Bao, W.-J.; Wang, F.-B.; Xia, X.-H. Catalyst-Free Synthesis of Nitrogen-Doped Graphene via Thermal Annealing Graphite Oxide with Melamine and Its Excellent Electrocatalysis. *ACS Nano* **2011**, *5*, 4350−4358.
(36) Jacobson, I. A.; Heady, H. H.; Dinneen, G. U. Thermal Reactions of Organic Nitrogen Compounds. I. 1-Methylpyrrole. *J. Phys. Chem.* **1958**, *62*, 1563−1565.
(37) Arrigo, R.; Havecker, M.; Schlogl, R.; Su, D. S. Dynamic Surface Rearrangement and Thermal Stability of Nitrogen Functional Groups on Carbon Nanotubes. *Chem. Commun.* **2008**, 4891−4893.
(38) Liang, H.-W.; Zhuang, X.; Brüller, S.; Feng, X.; Müllen, K. Hierarchically Porous Carbons with Optimized Nitrogen Doping as Highly Active Electrocatalysts for Oxygen Reduction. *Nat. Commun.* **2014**, *5*, 4973.
(39) Ma, Z.; Dou, S.; Shen, A.; Tao, L.; Dai, L.; Wang, S. Sulfur-Doped Graphene Derived from Cycled Lithium−Sulfur Batteries as a Metal-Free Electrocatalyst for the Oxygen Reduction Reaction. *Angew. Chem., Int. Ed.* **2015**, *54*, 1888−1892.
(40) Liu, R.; Wu, D.; Feng, X.; Müllen, K. Nitrogen-Doped Ordered Mesoporous Graphitic Arrays with High Electrocatalytic Activity for Oxygen Reduction. *Angew. Chem., Int. Ed.* **2010**, *49*, 2565−2569.
(41) Mayrhofer, K. J. J.; Strmcnik, D.; Blizanac, B. B.; Stamenkovic, V.; Arenz, M.; Markovic, N. M. Measurement of Oxygen Reduction Activities via the Rotating Disc Electrode Method: From Pt Model Surfaces to Carbon-Supported High Surface Area Catalysts. *Electrochim. Acta* **2008**, *53*, 3181−3188.

DOI: 10.1021/acsami.5b02902
ACS Appl. Mater. Interfaces 2015, 7, 14763−14769